

ATTITUDE AND HEADING REFERENCE SYSTEM
FOR SMALL UNMANNED AIRCRAFT COLLISION
AVOIDANCE MANEUVERS

KEVIN MURRANT



**Attitude and Heading Reference System for Small
Unmanned Aircraft Collision Avoidance
Maneuvers**

by

©Kevin Murrant

A thesis submitted to the School of Graduate Studies in partial fulfillment of the
requirements for the degree of

**Master of Engineering
Faculty of Engineering & Applied Science**

MEMORIAL UNIVERSITY OF NEWFOUNDLAND

May 2012

ST. JOHN'S

NEWFOUNDLAND

Abstract

This thesis describes the development of an Attitude and Heading Reference System (AHRS) to sense three-dimensional orientation for collision avoidance control in small unmanned aircraft. Unmanned aircraft are currently restricted to flight in designated airspace due to safety concerns of collision with manned aircraft. Therefore, collision avoidance is necessary to ensure the safety of both aircraft. Technical challenges, mainly in sensor limitations, restrict AHRS performance in attitude estimation during high- g maneuvers. Using sensor filtering techniques and a robust attitude representation, an AHRS suitable for collision avoidance is developed. Acceleration disturbances are reduced using estimates of non-gravitational accelerations including centripetal acceleration and model-based acceleration to improve gravity vector measurement during aircraft maneuvers. Simulation results with a variety of maneuvers deemed challenging for most AHRS are given showing accurate attitude estimates. Flight data from an existing commercial autopilot is compared with the results of the AHRS to demonstrate the validity of the solution with real flight data.

Acknowledgements

Thanks to my supervisors Dr. Siu O'Young and Dr. James Millan for their help and thanks to the RAVEN II team. Thanks to the project support from the Atlantic Canada Opportunities Agency's Atlantic Innovation Fund, and project partners Natural Sciences & Engineering Research Council of Canada, Research & Development Corporation of Newfoundland & Labrador, Provincial Aerospace Limited, and Defence Research & Development Canada.

Table of Contents

Abstract	ii
Acknowledgments	iii
Table of Contents	vi
List of Tables	vii
List of Figures	ix
List of Abbreviations	x
1 Introduction	1
1.1 Background	1
1.2 Problem Statement	2
1.2.1 Technical Difficulties	3
1.3 Expected Contributions	4
1.4 Organization	5
2 Background and Related Work	6
2.1 Attitude Representations	6
2.2 Filtering Methods	8

2.3	Model Aiding	11
2.4	AHRS Development	13
3	Theory	16
3.1	Preliminaries	16
3.1.1	Inertial sensors	17
3.1.1.1	MEMS Gyroscopes	17
3.1.1.2	MEMS Accelerometers	18
3.1.2	Notation and conventions	19
3.1.2.1	List of Symbols	20
3.2	AHRS Framework	21
3.2.1	Quaternion integration algorithm	22
3.2.2	Vector measurements	25
3.2.2.1	Wahba's problem	25
3.2.2.2	Attitude estimation	26
3.2.2.3	Centripetal acceleration correction	27
3.2.2.4	Aircraft model aiding	28
3.2.3	Extended Kalman filter	29
3.3	Original Contributions	32
3.3.1	Jacobian calculation	32
3.3.2	Logical constraints	34
3.3.2.1	Gravity versus orientation	34
3.3.2.2	Quaternion continuity	35
4	Simulation & Experimental Results	37
4.1	Simulation	37
4.1.1	MATLAB Simulation	39

4.1.1.1	Run A: smooth turns	40
4.1.1.2	Run B: turns with sharp transition	44
4.1.1.3	Run C: turns with sharp transition and airspeed increase	49
4.1.1.4	System identification of model parameters	54
4.1.1.5	Centripetal acceleration correction	57
4.2	Flight Test	60
5	Conclusion	63
5.1	Summary	63
5.1.1	Contributions	65
5.2	Future Work	66
	Bibliography	67

List of Tables

4.1	Inertial sensor noise figures	38
4.2	Simulation A input parameters	41
4.3	Simulation A error figures	44
4.4	Simulation B input parameters	45
4.5	Simulation B error figures	47
4.6	Simulation C input parameters	50
4.7	Simulation C error figures	53
4.8	Model correction error comparison for simulation	56
4.9	Simulation comparison with and without correction	59
4.10	AHRS versus MicroPilot attitude error	62

List of Figures

2.1 Kalman filter block diagram	9
3.1 Coriolis cross product diagram	18
3.2 Roll, pitch, and yaw definition	19
3.3 AHRS block diagram	22
3.4 EKF block diagram	30
4.1 Run A 3D perspective of attitude and trajectory	42
4.2 Run A true and estimated attitude angles	42
4.3 Run A attitude estimate error	43
4.4 Run A true and estimated gyro biases	43
4.5 Run A roll angles without gravity logic	45
4.6 Run B 3D perspective of attitude and trajectory	46
4.7 Run B true and estimated attitude angles	46
4.8 Run B attitude estimate error	48
4.9 Run B true and estimated gyro biases	48
4.10 Run B corrected and uncorrected accelerations	49
4.11 Run C 3D perspective of attitude and trajectory	51
4.12 Run C true and estimated attitude angles	51
4.13 Run C attitude estimate error	52

4.14 Run C true and estimated gyro biases	52
4.15 Run C attitude angles without inversion logic	53
4.16 Elevator to vertical acceleration system ID data	54
4.17 Elevator to vertical acceleration system ID results	56
4.18 Attitude plot for run B without model correction	57
4.19 Attitude plot for run A without correction	58
4.20 Attitude plot for run B without correction	59
4.21 MicroPilot reported and estimated attitude angles	61
4.22 Flight test attitude estimate error	61

List of Abbreviations

ACAS	Automatic Collision Avoidance System
AHRS	Attitude and Heading Reference System
ASAS	Automatic Separation Assurance System
CA	Collision Avoidance
DCM	Direction Cosine Matrix
GPS	Global Positioning System
IMU	Inertial Measurement Unit
INS	Inertial Navigation System
MEMS	Micro Electro-Mechanical Systems
PF	Particle Filter
RMS	Root Mean Square
TCAS	Traffic Collision Avoidance System
SS	Self Separation
sUA	Small Unmanned Aircraft
UKF	Unscented Kalman Filter

Chapter 1

Introduction

1.1 Background

Flight of small unmanned aircraft (sUA) is currently restricted to within line-of-sight from specially authorized runways by Transport Canada due to safety concerns of an aircraft or ground collision. Part of the solution to these safety concerns is known as sense and avoid. sUA must have the ability to sense obstacles and avoid them with every possible method of evasion, including self-destruction. The ability to sacrifice the unmanned aircraft provides a unique advantage to sUA versus paramount survival for manned aircraft during collision avoidance (CA).

sUA can perform high- g maneuvers in any attainable orientation, whereas human pilots can become unconscious in situations where the acceleration approaches 5 g , as stated in the work by Beaudette [1]. The advantage of sUA for maneuvering more aggressively than manned aircraft is an encouraging point for CA. sUA can likely and potentially avoid predicted collisions with less available response time than manned aircraft.

There is a distinction made between airborne collision avoidance systems (ACAS)

and airborne separation assurance systems (ASAS), intended for CA and self-separation (SS), respectively. To maintain SS, rules governing right of way are applied. However, CA is an emergency situation and any maneuver can be employed to prevent a collision. Collision is defined as physical contact while separation has varying definitions depending on the application. For example, the Traffic Collision Avoidance System (TCAS) [2], is designed for commercial air traffic while FLARM [3] is intended for smaller aircraft, in particular gliders, which can be in close proximity without danger of collision. Most, if not all, of these systems are transponder-based and alert the pilot to take action with some information about the threat. In some cases there are guidelines for avoidance maneuvers. However, defining the quantitative distinction between SS and CA is outside the scope of this thesis, but is discussed in a paper by Van Gent et al. [4]. SS is intended to avoid CA encounters with a subtle maneuver or course alteration. In the event of a CA encounter, sUA require an automatic maneuver to avoid the intruder. The CA control requires an attitude and heading reference system (AHRS) capable of providing accurate feedback throughout the maneuver.

The attitude and heading must be detected electronically and the nature of the platform limits resources available in terms of size, weight, power consumption, and cost. Making use of hardware that meets these criteria, the software is key to tracking the attitude and heading despite sensor flaws or complex trajectories. Therefore, existing methods for attitude and heading estimation, such as attitude representation and filtering, must be tailored to the CA requirements of sUA.

1.2 Problem Statement

The goal of this thesis is to develop an AHRS that fulfills automatic CA maneuver sensor requirements for high- g motion in any orientation.

1.2.1 Technical Difficulties

Sensor limitations are the main difficulty in achieving an accurate attitude and heading estimate. Gyroscopes have an inherent bias that requires integration, resulting in an orientation error that grows with time, along with other sources of error such as rate limitation, non-linearity, and crosstalk, though these are less critical. The bias integration error must be corrected with a non-integrating source of orientation measurement, in most cases gravity and Earth's magnetic field. Accelerometers suffer from similar sources of error as gyroscopes, but more importantly, non-gravitational accelerations are a large disturbance to the measurement of gravity. Likewise, magnetic measurements are subject to disturbances in the local magnetic field.

The secondary difficulty in developing an AHRS specifically for CA is in the mathematical representation of the attitude and the smooth resolution of the vector measurements into this attitude representation.

These difficulties exist for any AHRS development. For CA maneuvering, it is advantageous that as few restrictions as possible be placed on the types of available maneuvers. Technically, this can be interpreted as any trajectory possible with the airframe, or any possible orientation and rate. Therefore, two aspects are crucial: the attitude representation and removing non-gravitational accelerations, while remaining within sensor saturation limits. However, the latter is considered a low concern as the sensor range is generally sufficient. There is also a connection between the attitude representation and removal of non-gravitational accelerations involving the mechanization¹ of the vector attitude measurements. The vector attitude measurement must be independent of the orientation which is not the case with many common methods, e.g. simple trigonometric calculation, but this issue has been addressed in

¹Mechanization is a term originating from gimbaled INS, which are mechanically stabilized in the inertial frame, essentially what is done mathematically in a strapdown INS.

spacecraft attitude determination and solutions can be applied here.

In summary, the main technical difficulties are:

1. Gyroscope bias integration error,
2. Gravity measurement obscured by non-gravitational accelerations,
3. Magnetic field distortions affecting compass measurement, and
4. Resolving gyroscope and vector measurements into a common, unique attitude representation.

1.3 Expected Contributions

To achieve the goal of creating an AHRS for CA applications in sUA, the previously stated technical challenges must be overcome. The expected contributions from solving these technical challenges include the integration of various existing methods in filtering, attitude representation, and disturbance estimation. This integration requires the following original work:

1. Quaternion-based Extended Kalman filter (EKF) integrated with vector attitude measurements using logical constraints to ensure reliability,
2. Derivation of Jacobian matrix for quaternion rate integration with gyroscope biases in the state vector,
3. Application of centripetal and model-based acceleration correction for an improved estimate of the gravity vector, and
4. Development of a closed-loop simulation to verify results.

1.4 Organization

This thesis is organized as follows: in Chapter 2, an overview of the literature is provided regarding AHRS development, mainly in terms of attitude representation, filtering techniques, and aiding sources. In Chapter 3, the theory required to create an AHRS is presented, beginning with an introduction to the sensors used, then an overview of the mathematics behind the quaternion representation of aircraft attitude and EKF, and finally an overview of the practical constraints used in the system. The preparation and results from MATLAB simulation, which comprise the majority of the results, are found in Chapter 4. This chapter also contains the results from using recorded flight data and compares the results with those of another autopilot. The conclusions from the AHRS development, contributions, and future work are given in Chapter 5.

Chapter 2

Background and Related Work

2.1 Attitude Representations

An extensive review of modern attitude representations is given in the survey paper by Shuster [5], a summary of which follows.

Rotation matrices are the standard for comparison with other representations. Rotations are represented by 3×3 matrices, therefore dimension 9, and form what is called the special orthogonal group in 3 dimensions, or $SO(3)$ as referred to in related literature using this attitude representation, such as the work by Mahony et al. [6], and also applied to sUA by Euston et al. [7]. There are various methods for composing rotation matrices, one popular method is direction cosines. With this method, the resulting rotation matrix is usually referred to as a direction cosine matrix (DCM). This is a common attitude representation used, for example, by Edwan et al. [8].

The most familiar attitude representation is Euler angles. This representation has minimum dimension 3 but is computationally burdensome compared to rotation matrices and singularities exist for certain rotations. Hence this representation is rarely used for attitude tracking. Euler angles are the representation of choice when

it comes to human interpretation of the attitude and, as such, are used in all attitude plots in the subsequent chapters.

Similar to Euler angles is the Axis-Azimuth representation which is defined as a rotation about an axis. The representation uses 3 angles: two to define the elevation and right-ascension of the axis, respectively, and a third angle to define the rotation about that axis. This representation is of particular use in application to spinning spacecraft and is described by Wertz [9]. This representation is interesting as a unique geometric interpretation for CA may be possible. Another parameterization of the Axis-Azimuth representation is a vector \mathbf{t} defined in the reference frame where the magnitude t defines the angle to be rotated about the axis to align the frame of interest into the reference frame.

Another attitude representation is known as Euler-Rodrigues symmetric parameters or, more commonly, the quaternion of rotation. Altmann [10] gives an interesting account on the origins of this representation. The quaternion of rotation is dimension 4, which is the minimum dimension required to avoid any singularities. Besides this advantage of compactness over rotation matrices, quaternions of rotation also feature a simple composition rule for successive rotations and have only one constraint versus six constraints for rotation matrices. That is, the quaternion of rotation must have a total magnitude of unity, whereas rotation matrices must maintain orthogonality. Therefore, the constraint is much easier to impose. Due to these qualities, this is the representation used in Chapter 3 and also by Bar-Itzhack and Oshman [11], Choukroun et al. [12], Hall et al. [13], and Marins et al. [14], in each of which the quaternion is a main aspect of the work. In terms of the vector \mathbf{t} for the Axis-Azimuth representation, a quaternion representation can be derived as in Equation 2.1, from Section 3.6.4.1 of Titterton and Weston [15].

$$\hat{Q} = \begin{bmatrix} q_0 \\ q_1 \\ q_2 \\ q_3 \end{bmatrix} = \begin{bmatrix} \cos(t/2) \\ (t_x/t)\sin(t/2) \\ (t_y/t)\sin(t/2) \\ (t_z/t)\sin(t/2) \end{bmatrix} \quad (2.1)$$

where t_x, t_y, t_z are the components of the angle vector \mathbf{t} .

There are also some variations on quaternions of rotation such as the Gibbs vector, in which the normalization constraint is implicit and the dimension reduced to 3. However, these variations result in more complication than the Euler-Rodrigues symmetric parameters and are excluded here.

Shuster [5] also goes on to describe the attitude kinematics for each representation. This is the relationship between the temporal derivative of the attitude representation and the angular velocity, which is required for integration of the gyroscope rates into the attitude estimate. In summary, the quaternion of rotation representation is chosen for use in Chapter 3 as it has the least restriction versus any of the other attitude representations.

2.2 Filtering Methods

To reduce error in the attitude estimate, regardless of attitude representation, filtering must be applied. Filtering, in this context, refers not only to the reduction of noise but the fusion of attitude estimates from various sources. In general, these sources include a high-rate attitude estimate from angular rate integration and a low-rate attitude estimate from a non-integrating source. AHRs and INS have long benefited from the work of Kalman [16], who introduced the Kalman filter. The Kalman filter generates a statistically optimal estimate of the state of a system given a linear model

of the system dynamics and noisy measurements of the output. A block diagram of the linear Kalman filter is shown in Figure 2.1 and is from Appendix A of Titterton and Weston [15].

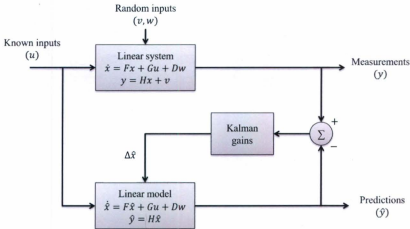


Figure 2.1: Block diagram of linear Kalman filter.

In terms of Figure 2.1, the system under consideration is assumed linear and contaminated by Gaussian noise w . The output of the system y is a linear combination of the state vector x with additional Gaussian noise v . The Kalman filter uses a model of the system with knowledge of the system and measurement noise statistics (in the form of covariance matrices Q and R , respectively) to generate an estimate of the state \hat{x} . The output is predicted using the state estimate and compared with the measurement. The difference is weighted by the Kalman gain to provide a best estimate correction to the estimated state vector in a least-squares sense. The Kalman gain is updated with each time step according to the calculated process covariance P . Further details of the Kalman filter equations are given in Section 3.2.3 which covers

the EKF, a non-linear extension of the Kalman filter.

The attitude kinematics, which compose the system model for an AHRS filter, are generally non-linear. Therefore, non-linear filtering methods must be considered. A survey of non-linear filtering methods is given by Crassidis et al. [17], from which a summary of relevant points follows.

The EKF is the most common non-linear estimator. It works much like the linear Kalman filter described above, except the system model is linearized with a first-order approximation using the current state estimate. Variations of the EKF are also common, depending on the application. For example, the multiplicative EKF which represents the attitude as the product of an attitude estimate and a small deviation from that attitude, the advantage being that the deviation cannot reach a singularity as it is small. This method was used, for example, in the work by Murrell [18] for NASA. Many of the variations relate to how the state vector is chosen, but the most straight-forward method is to simply include a non-singular attitude parameterization in the state vector, as done in Section 3.2.3.

Another common attitude determination method is known as QUEST and was introduced by Shuster and Oh [19]. This method determines the attitude based on vector measurements and is similar to the method used in Section 3.2.2.2 for the non-integrating measurement. The method was later extended to a filter by Shuster [20] for when an estimate is required over a period of observations rather than an instant, but the Kalman filter has seen more use in practice.

Among the remaining non-linear filtering methods of interest are the Unscented Kalman Filter (UKF) and Particle Filters (PF). The UKF is based on the principle that it is easier to estimate a Gaussian probability distribution versus a non-linear function. This method has seen some popularity in AHRS development such as the work by Pourtakdoust and Asl [21] and Huimin and Wenyong [22], which are re-

cent attitude filters based on the UKF. PF are methods that have come about from increased availability of computational power: they have the advantage of being optimal estimators for both non-linear and non-Gaussian systems. This method has been used for attitude determination, for example, by Cheng and Crassidis [23]. The disadvantages of PF include computational burden and complex implementation. As mentioned in the introduction, the UKF was considered, but the performance was found to be nearly identical to that of the EKF, which was chosen to reduce implementation complexity.

Crassidis et al. [17] describes some other non-linear filtering methods in the survey paper, which are not mentioned here, but the conclusion of the paper is that the EKF is still the standard for attitude determination. As the focus is not to improve filtering methods but improve performance during CA maneuvers, the standard quaternion-based EKF was chosen as the core of the AHRS.

2.3 Model Aiding

In recent years, aiding of inertial sensing with dynamics modeling has become a popular research topic, particularly for ground and surface marine vehicles, which have more motion constraints than aircraft. For example, under normal operation a car can only travel in the direction the tires are pointing, it cannot move sideways. A general purpose INS can report motion perpendicular to the tires from drift or acceleration disturbance, or vertical motion despite the vehicle being on the ground. If the vehicle dynamics were considered, this reported motion could be constrained. An aircraft is not constrained in any direction of motion, but is governed by certain dynamics which can be estimated with a model to improve navigation performance.

One of the first papers specifically on INS aiding with aircraft dynamics is by

Koifman and Bar-Itzhack [24]. These authors used a full aircraft dynamics model and INS separately and used an EKF to correct the errors in each from the difference in the two estimates of the position, velocity, and attitude. The paper reports success in improving the overall performance of low-grade INS. A similar paper, also reporting successful INS improvement, focusing on underwater vehicles was published by Hegrenæs et al. [25]. Another similar paper was written for land vehicles by Ma et al. [26]. Using a full dynamics model for UAV with low-cost sensors was described in a paper by Bryson and Sukkarieh [27] with promising simulation results.

Embedded vehicle model aiding where the model is part of the EKF was considered in a paper by Vasconcelos et al. [28]. The authors report equivalent success in using the embedded model versus external aiding with the advantage of a computational savings by including the INS states in the model filter.

Use of a full dynamics model in real-time requires a lot of computational power and for AHRS alone, a full model is not necessary. Euston et al. [7] use a first-order model to estimate angle of attack dynamics based on pitch rate. This is a similar approach to the model aiding used in Section 3.2.2.4 to estimate non-gravitational acceleration using elevator input instead of pitch rate. It may be possible to estimate angular rates if necessary, but non-gravitational acceleration estimation is the most valuable aspect of model aiding to develop an AHRS for CA. However, model aiding requires customization for each application, depending on the airframe and environment. This requires previous system identification or on-line identification which identifies the model parameters during flight.

2.4 AHRS Development

AHRS refers specifically to a system to detect the attitude, or pose, of an aircraft, and the heading. This differs from an Inertial Navigation System (INS) as only an estimate of the attitude and heading is made and there is no extension to position and velocity. Modern AHRS are referred to as strapdown, meaning the sensors are rigidly attached to the platform and the inertial frame is determined mathematically. In the past, gyroscopes were mechanically stabilized in the inertial frame. Development of an AHRS specifically for CA has not been done before, but existing AHRS may already suffice for CA. Many high-end AHRS are used in military applications, such as missile guidance, and are not available for comparison. It is likely that they exceed the requirements for CA. However, the cost of these high-end AHRS is very high and prohibitive for low-cost sUA. The low-cost AHRS make use of filtering to estimate gyroscope biases and correct errors to offset the relatively low accuracy of the sensors used. The accuracy of the AHRS estimates in the low-cost case varies depending on the implementation and sensor quality.

A basic AHRS design is described by da Paixao et al. [29] which uses DCM, or rotation matrix, for attitude representation and is implemented in hardware. The authors do not mention acceleration correction, and only desktop IMU results are given. These results are not indicative of real flight due to the absence of constant non-gravitational accelerations from aircraft maneuvering.

Another design similar to that described in Chapter 3 is outlined by Guerrero-Castellanos et al. [30]. Quaternions are used but with a multiplicative EKF which considers small deviations in attitude. Again, no mention was made of acceleration correction, and the results are not representative of a CA maneuver.

Gebre-Egziabher et al. [31] describe both a Euler angle and quaternion based AHRS with good results. These authors use a Global Positioning System (GPS)

based attitude determination system as an aiding source. The GPS based attitude determination is noisy and requires a larger airframe to separate the antennas to increase the resolution between the GPS measurements and is therefore not applicable to sUA.

Two more AHRS designs are described by Munguia and Grau [32] and Batista et al. [33]. The first is quaternion-based using two EKF: one for updating attitude kinematics and another for estimating gyroscope biases based on the error. The results do not indicate a truth measurement for attitude and are not really indicative of the performance. The other AHRS is unique as it lacks an attitude representation. The sensor measurements are filtered directly, and the attitude is calculated from the filtered sensor measurements. This method avoids the problems associated with attitude representation such as singularities, but there is no focus on attitude estimation during high- g maneuvers. The experimental results are based on a calibration device and they are not conclusive for CA.

Finally, Ryan and Miller [34] describe the development of an AHRS as a replacement for high-rate sensors for a gimballed camera system. They do not have many results of the actual AHRS performance, and the application is not for aircraft. However, the focus on using a low-cost AHRS as a replacement for more expensive high-rate sensors is in line with the focus of CA for sUA. The authors conclude that they are able to meet the performance requirements of the gimballed camera with a significant reduction in cost.

Other AHRS designs exist, but some are commercial products and not described in academic literature. However, it is clear that many authors do not consider the effects of high- g maneuvers on AHRS performance. Currently, much of the focus is on optimizing attitude representation, improving filtering methods, or developing a new configuration of these two or more methods. This can result in a reduction of

theoretical error but, for high- g maneuvers using MEMS-based sensors, the numerical accuracy is unimportant compared to reducing error during significant motion. Therefore, the use of the quaternion attitude representation and EKF, which are proven AHRS methods, is coupled with non-gravitational acceleration estimation techniques to reduce the error during these maneuvers. The theory and specification of the mathematics behind the AHRS developed in this thesis is presented in the next chapter.

Chapter 3

Theory

This chapter is organized with a brief introduction followed by a detailed description of the equations required for an AHRS. The innovations required to satisfy the requirements of CA are described in the final sections.

3.1 Preliminaries

In this chapter, the mathematical framework and description of the sensors required to create a functional AHRS are described. The following sections up to Section 3.3 contain previous work developed by others, summarized here using consistent notation. As this thesis is focused on creating an AHRS for use in CA, many of the design decisions in terms of attitude representation and acceleration correction are directed towards this end. The focus is on using low-cost sensors with the best possible software algorithms to create a robust solution to the sensor requirement for CA. An overview of inertial sensors, notation, and conventions follows.

3.1.1 Inertial sensors

Two types of true inertial sensors are used for most AHRS: gyroscopes to sense angular rate, and accelerometers to sense acceleration. The term gyroscopes implies angular rate sensors, contrary to the traditional differentiation between rate gyroscopes and gyroscopes which reported attitude angles. The two are discussed further in the following subsections, where this information is restated from Titterton and Weston [15]. These sensors alone cannot give a reliable heading. Therefore, it is necessary to include a magnetometer to create a complete AHRS. Technically, the magnetometer is not an inertial sensor, but is often included as part of an IMU. The Micro Electro-Mechanical Systems (MEMS) grade of sensors is considered here, as the cost of high-end sensors which operate on different principles is usually prohibitive for use in sUA outside of military applications.

3.1.1.1 MEMS Gyroscopes

MEMS gyroscopes operate on the principle of the Coriolis acceleration effect on a vibrating proof mass, which is given by Equation 3.1.

$$a_{\text{cori}} = 2V \times \Omega \quad (3.1)$$

where V is the velocity and Ω is the rate of rotation around the sensing axis. This equation is illustrated in Figure 3.1.

The proof mass is in vibrating oscillatory motion along an axis perpendicular to that of the sensing axis. From the cross product in Equation 3.1, the coriolis acceleration is perpendicular to both the sensing axis and the direction of motion. The acceleration is detected and with previous knowledge of the velocity of oscillation, the rate of rotation can be calculated.

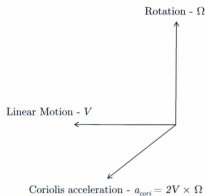


Figure 3.1: Diagram of Coriolis force cross product.

This simple design is susceptible to external disturbances, however, and in most modern designs a balanced tuning fork design is used. This design uses a balanced oscillator to reduce the effect of external disturbances. This is simplified compared to what is actually in production MEMS gyroscopes, but the basic principle is the same for most gyroscopes based on the tuning fork design.

3.1.1.2 MEMS Accelerometers

MEMS accelerometers operate based on the mechanical properties of the materials from which they are constructed, which is almost exclusively silicon. There are two main classes of MEMS accelerometers. The pendulous mass accelerometer detects acceleration by sensing the displacement of a proof mass suspended by a hinge in the presence of an applied acceleration. The other class of MEMS accelerometer is based on the principle that the vibrational frequency will change when a mechanical loading is applied due to the acceleration along the sensing axis. The design choices for each of these classes determines the operating range. For example, the pendulous mass

accelerometer must be rotationally displaced versus its hinge and there is clearly a limited range to this type of rotation. The resonating accelerometer has limits on its operating range due to the mechanical limitations of the material and structure. Other types of MEMS accelerometers exist but these are the two most common and popular designs.

3.1.2 Notation and conventions

Inertial navigation and aeronautics in general is inconsistent in notation. Most notation for inertial systems follows conventions such as those proposed by Britting [35]. There is also an IEEE Standard for Inertial Systems Terminology [36] which contains many useful definitions and some quaternion notation.

The sign convention used in most of this development and the definition of the positive roll ϕ , pitch θ , and yaw ψ angles is shown in Figure 3.2.

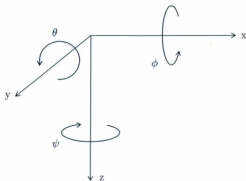


Figure 3.2: Definition of roll, pitch, and yaw angles.

When referring to the angular rates associated with each axis, the axis name is used as a subscript. For example, ω_x refers to an angular rate about the x -axis, affecting the roll ϕ .

The attitude representation used in this thesis is the quaternion of rotation or Euler-Rodriguez parameters. These are a subset of the quaternion as the quaternion of rotation must have a modulus of 1, whereas the quaternion itself does not have this constraint. However, quaternion is used in this thesis to represent the quaternion of rotation. The IEEE Standard for Inertial Systems Technology recommends the following terminology for quaternions:

$$\bar{Q} = [\lambda, \rho] = \begin{bmatrix} q_0 & q_1 & q_2 & q_3 \end{bmatrix} \quad (3.2)$$

where λ or q_0 represent the scalar part of the quaternion and ρ represents the vector part. The quaternion components are used in this thesis as they form part of the state vector.

3.1.2.1 List of Symbols

A brief list of symbols excluding those explicitly defined in this chapter:

ϕ	Roll angle	\mathbf{a}_c^b	Body-frame centripetal acceleration
θ	Pitch angle	\mathbf{g}^b	Body-frame gravity measurement
ψ	Yaw angle	\mathbf{g}^n	Navigation-frame gravity vector
ω	Angular rate vector	\mathbf{m}^b	Body-frame magnetometer measurement
\bar{Q}	Quaternion of rotation	\mathbf{m}^n	Navigation-frame magnetic reference vector
q	Quaternion component	$\boldsymbol{\mu}$	Gyroscope bias vector
Δt	Calculation time-step	$\hat{\mathbf{x}}$	Estimated state vector
\mathbf{v}	Body-frame velocity	\mathbf{u}	Input vector
v_a	Airspeed		

3.2 AHRS Framework

The basis of strapdown AHRS is the mathematics used to condition the sensor readings to obtain an accurate solution of attitude and heading. A block diagram of the AHRS algorithm developed in this thesis is shown in Figure 3.3. Generally, two sources of measurement are used to develop the attitude and heading solution. Gyroscopes provide the high-rate measurement which is integrated to determine the angle of rotation. However, from this integration, these measurements suffer from drift due to bias in the sensor readings. To correct this drift, another source of measurement is used which does not require integration. Vector measurements in the body frame are made of quantities known in the navigation frame and attitude is calculated by determining the rotation required to align the vectors. For example, a three dimensional measurement of acceleration will contain gravitational acceleration which is known to be directed downwards. At least two vector measurements are required to obtain a unique solution. In this case, the Earth's gravity and it's magnetic field are used as the reference vectors. These vector measurements are considered low-rate compared to the gyroscope integration.

The EKF achieves three objectives: sensor fusion, noise rejection, and gyroscope bias estimation. Sensor fusion, in this case, refers to the creation of an estimate based on the integrated angular rates and the vector attitude measurement. The gyroscope biases are then estimated to minimize the error between the two measurements. The EKF principle of operation is described in Chapter 2. The state transition function, or model, used by the EKF is the quaternion integration algorithm described in Section 3.2.1. The EKF itself is described in more detail in Section 3.2.3. Using this method alone, a good estimate of the attitude and heading can be obtained.

The main source of error is due to non-gravitational acceleration corrupting the gravity measurement. This is particularly a problem during the high- g maneuvers

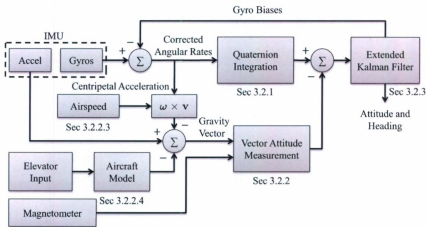


Figure 3.3: Block diagram of attitude and heading reference system.

being considered in this thesis. Therefore, removing non-gravitational acceleration from the accelerometer output before calculating the low-rate attitude and heading measurement is a priority. Two corrections are made to the accelerometer output to improve the accuracy of gravity in the measurement: the centripetal acceleration shown in Figure 3.3 from the corrected angular rates, and an estimate of the translational acceleration in the body frame obtained via an aircraft dynamics model and elevator input signal multiplied by the squared airspeed. Each component of the system is explained in more detail in the following subsections.

3.2.1 Quaternion integration algorithm

The quaternion of rotation is updated with gyroscope rate information at each time step using the quaternion integration algorithm as given in Section 11.2.5 of Titterton and Weston [15]. The matrix form of the integration equation is:

$$\frac{d\tilde{Q}}{dt} = \frac{1}{2}\mathbf{W}\tilde{Q} \quad (3.3)$$

where

$$\mathbf{W} = \begin{bmatrix} 0 & -\omega_x & -\omega_y & -\omega_z \\ \omega_x & 0 & \omega_z & -\omega_y \\ \omega_y & -\omega_z & 0 & \omega_x \\ \omega_z & \omega_y & -\omega_x & 0 \end{bmatrix} \quad (3.4)$$

and ω_x , ω_y , and ω_z are the components of $\boldsymbol{\omega}$. Equation 3.3 is well-known and forms the basis for strapdown inertial navigation systems using the quaternion attitude representation.

If the orientation of the rate vector, $\boldsymbol{\omega}$, remains fixed over the update interval, the above equation can be discretized as:

$$\tilde{Q}_{k+1} = \exp\left[\frac{1}{2}\int_{t_k}^{t_{k+1}} \mathbf{W} dt\right] \tilde{Q}_k \quad (3.5)$$

The integral can be rewritten

$$\int_{t_k}^{t_{k+1}} \mathbf{W} dt = \Sigma = \begin{bmatrix} 0 & -\sigma_x & -\sigma_y & -\sigma_z \\ \sigma_x & 0 & \sigma_z & -\sigma_y \\ \sigma_y & -\sigma_z & 0 & \sigma_x \\ \sigma_z & \sigma_y & -\sigma_x & 0 \end{bmatrix} \quad (3.6)$$

where $\boldsymbol{\sigma} = \Delta t \boldsymbol{\omega}$, which gives

$$\tilde{Q}_{k+1} = \exp\left(\frac{\Sigma}{2}\right) \tilde{Q}_k \quad (3.7)$$

The matrix exponential can be expanded and written as a quaternion product, the

derivation details of which are given in the reference above, to give:

$$\bar{Q}_{k+1} = \bar{Q}_k \otimes \bar{Q}_{AB} \quad (3.8)$$

where \otimes represents the quaternion product and \bar{Q}_{AB} is the quaternion of rotation from coordinate system (A), the body axes at time t_k , to coordinate system (B), the body axes at time t_{k+1} , and is given by:

$$\bar{Q}_k = \begin{bmatrix} a_c & a_x \sigma_x & a_y \sigma_y & a_z \sigma_z \end{bmatrix}^T \quad (3.9)$$

$$a_c = \cos\left(\frac{\sigma}{2}\right) \quad (3.10)$$

$$a_s = \frac{\sin(\sigma/2)}{\sigma} \quad (3.11)$$

and

$$\sigma^2 = (\sigma_x^2 + \sigma_y^2 + \sigma_z^2) \quad (3.12)$$

This is the algorithm used in this thesis for the quaternion integration. However, the following third-order expansion¹ is used for calculation of a_c and a_s :

$$a_c = 1 - \frac{(0.5\sigma)^2}{2!} \quad (3.13)$$

$$a_s = 0.5 \left(1 - \frac{(0.5\sigma)^2}{3!} \right) \quad (3.14)$$

and the estimated gyroscope bias vector $\boldsymbol{\mu} = [\mu_x \mu_y \mu_z]^T$ is subtracted from the rate vector $\boldsymbol{\omega}$ prior to calculation.

¹Table 11.2 in Titterton and Weston [15] shows that expansion beyond third-order is unnecessary given the intended sensor resolution used in this application.

3.2.2 Vector measurements

The vector measurements include gravity and magnetic field. The gravity reference is assumed to be straight down in the navigation frame. Given the limited range of the sUA considered in this thesis, this assumption is valid. The magnetic field reference is determined either by an almanac or calibration procedure.

The accelerometers and magnetometers provide two measured unit vectors \mathbf{g}^b and \mathbf{m}^b in the body frame. The components of the two corresponding vectors gravity \mathbf{g}^n and magnetic \mathbf{m}^n in the navigation frame are also known. The goal is to find the quaternion representation of the rotation matrix A such that:

$$A\mathbf{g}^n = \mathbf{g}^b \quad (3.15)$$

$$A\mathbf{m}^n = \mathbf{m}^b \quad (3.16)$$

This type of problem was first posed by Wahba [37] in 1965.

3.2.2.1 Wahba's problem

The problem, restated by Markley [38], is to find the rotation matrix A that minimizes the loss function:

$$L(A) := \pm \sum_i a_i |\mathbf{b}_i - A\mathbf{r}_i|^2 \quad (3.17)$$

where $\{\mathbf{b}_i\}$ is a set of n unit vectors in the body frame, $\{\mathbf{r}_i\}$ is a set of n unit vectors in the reference frame, and $\{a_i\}$ is a set of non-negative weights.

There have since been many solutions to this problem, as stated in the above reference. Of particular use to this thesis are the solutions which solve for the quaternion representation of the rotation matrix A . The following section describes the chosen solution.

3.2.2.2 Attitude estimation

The optimal quaternion estimation method detailed by Markley [38] was chosen as the solution to the previously described problem. This is due to the inherent use of the quaternion of rotation and the optimality of the solution. The computational load of this optimal method is not a burden on modern microprocessors and therefore there is little reason to consider suboptimal methods. Alternatives to this solution exist, but do not offer significant advantages over this method.

The algorithm derivation are given in the above reference, with the essential details as follows, using the notation introduced above for this application. The following normalized cross products simplify the solution:

$$\mathbf{r}_3 := \frac{(\mathbf{g}^n \times \mathbf{m}^n)}{|\mathbf{g}^n \times \mathbf{m}^n|} \quad (3.18)$$

$$\mathbf{b}_3 := \frac{(\mathbf{g}^b \times \mathbf{m}^b)}{|\mathbf{g}^b \times \mathbf{m}^b|} \quad (3.19)$$

Given the weights a_1 and a_2 for the gravity and magnetic measurements, respectively, the following intermediate quantities are defined:

$$\alpha := (1 + \mathbf{b}_3 \cdot \mathbf{r}_3) (a_1 \mathbf{g}^b \cdot \mathbf{g}^n + a_2 \mathbf{m}^b \cdot \mathbf{m}^n) + (\mathbf{b}_3 \times \mathbf{r}_3) \cdot (a_1 \mathbf{g}^b \times \mathbf{g}^n + a_2 \mathbf{m}^b \times \mathbf{m}^n) \quad (3.20)$$

$$\beta := (\mathbf{b}_3 + \mathbf{r}_3) \cdot (a_1 \mathbf{g}^b \times \mathbf{g}^n + a_2 \mathbf{m}^b \times \mathbf{m}^n) \quad (3.21)$$

$$\gamma := \sqrt{\alpha^2 + \beta^2} \quad (3.22)$$

The estimate is then computed as either:

$$\hat{Q} = \frac{1}{2\sqrt{\gamma(\gamma + \alpha)}(1 + \mathbf{b}_3 \cdot \mathbf{r}_3)} \begin{bmatrix} (\gamma + \alpha)(\mathbf{b}_3 \times \mathbf{r}_3) + \beta(\mathbf{b}_3 + \mathbf{r}_3) \\ (\gamma + \alpha)(1 + \mathbf{b}_3 \cdot \mathbf{r}_3) \end{bmatrix} \text{ for } \alpha \geq 0 \quad (3.23)$$

or

$$\tilde{Q} = \frac{1}{2\sqrt{\gamma(\gamma - \alpha)(1 + \mathbf{b}_3 \cdot \mathbf{r}_3)}} \begin{bmatrix} \beta(\mathbf{b}_3 \times \mathbf{r}_3) + (\gamma - \alpha)(\mathbf{b}_3 + \mathbf{r}_3) \\ \beta(1 + \mathbf{b}_3 \cdot \mathbf{r}_3) \end{bmatrix} \text{ for } \alpha \leq 0 \quad (3.24)$$

As commented by Markley [38], the overall sign of \tilde{Q} is irrelevant because there is a quadratic relation between \tilde{Q} and the rotation matrix A and therefore has no effect on the solution to the problem as originally stated. However, the overall sign is important in the filtering stages, and this is discussed further in Section 3.3.2.2. This method requires that the two reference vectors are not colinear, which is normally the case on Earth. Also, there is a singularity condition if $\mathbf{b}_3 = -\mathbf{r}_3$ which can be avoided by solving for the attitude in a reference frame rotated 180° from the original reference frame and then rotating the solved attitude back to the original reference frame.

3.2.2.3 Centripetal acceleration correction

A component of the acceleration detected by the accelerometers is the centripetal acceleration experienced during turning maneuvers. Of particular interest are banked turns, during which the normalized gravity reading is biased by the centripetal acceleration. In the case of a horizontal banked turn, this results in an incorrect estimate of the roll angle.

To correct for this error, the centripetal acceleration can be estimated and removed from the accelerometer output. The centripetal acceleration can be calculated as in Hibbeler [39], or any dynamics text:

$$\mathbf{a}_c = \boldsymbol{\omega} \times (\boldsymbol{\omega} \times \rho \mathbf{r}) \quad (3.25)$$

where ρ is the radius of the turn and \mathbf{r} is a unit vector towards the center of the turn. The radius of the turn is normally not known, but can be estimated with GPS. In this thesis, however, GPS is avoided and the centripetal acceleration can be estimated by assuming $\boldsymbol{\omega} \times \rho \mathbf{r}$ can be approximated by the airspeed v_a as done by Euston et al. [7]. The airspeed is assumed to be along the x -axis of the aircraft. The x -axis component of the groundspeed is required when considering the effect of wind, but the airspeed is equivalent in the absence of wind. This results in the following equation for centripetal acceleration:

$$\mathbf{a}_c^b = \boldsymbol{\omega} \times \mathbf{v} \quad (3.26)$$

where

$$\mathbf{v} = \begin{bmatrix} v_a & 0 & 0 \end{bmatrix}^T \quad (3.27)$$

Test results indicate that this is a valid approximation for the centripetal acceleration, as will be shown in subsequent chapters. However, it is necessary to reverse the overall sign of the centripetal acceleration term during inverted flight. This is because only the scalar speed is used for the approximation rather than the vector towards the center of the turn, which would be reversed during inverted flight. This is handled similarly to the gravity correction in Section 3.3.2.1.

3.2.2.4 Aircraft model aiding

The only detectable non-gravitational acceleration term remaining is due to translational accelerations in the body frame of the aircraft. The body frame velocities of the aircraft are referred to by Phillips [40] as u, v, w for the x, y, z axes, respectively, where the x -axis is aligned along the center-line of the aircraft. Therefore, the body frame translational accelerations are given by $\dot{u}, \dot{v}, \dot{w}$. Unfortunately, there is no accurate way to measure the body frame velocities.

Simulation results have shown that the vertical component of the acceleration can be estimated using the control signal for the elevator. It can be derived from flight mechanics (such as the text by Phillips [40]) that the total vertical acceleration is proportional to the rate of change of the pitch angle. Also, the rate of change of the pitch angle is proportional to the elevator deflection angle, which is clearly proportional to the elevator control signal. The proportionality is dependent on the squared airspeed, v_a^2 , of the aircraft. From simulation, where all quantities are known precisely, it has been found that the elevator control signal is proportional to the remaining vertical translational acceleration term. Using δ_e to represent the elevator control signal, and $a_{t,z}$ as the remaining vertical translational acceleration term:

$$\delta_e v_a^2 \propto a_{t,z} \quad (3.28)$$

By using system identification techniques such as those described in Ljung [41], it is possible to identify a model which can accurately predict $a_{t,z}$ for use as a correction term to be removed from the accelerometer output. Simulation and system identification methods have shown that a 2nd-order state-space model results in an accurate fit of the data for the MATLAB simulation. This method may be less effective for a manually controlled flight, as there is no coupling between the altitude and speed via the controller. The coupling in this case is due to the nature of the controller used for the simulation, which controls the altitude using the throttle.

3.2.3 Extended Kalman filter

The quaternion rate integration and vector attitude measurement are fused to create a filtered estimate using the EKF². The state transition function f is non-linear and

²The unscented Kalman filter was also considered, but filtering performance was found to be identical to the EKF, and because the Jacobian matrix was known exactly it was more straightforward

the EKF linearizes f about the current state to update the process covariance using a first-order approximation. The state is predicted using the previous state and input signals with a model of the system dynamics. This state prediction is then corrected with the attitude measurement information. A block diagram of the EKF is given in Figure 3.4 which is adapted from Welch and Bishop [42].

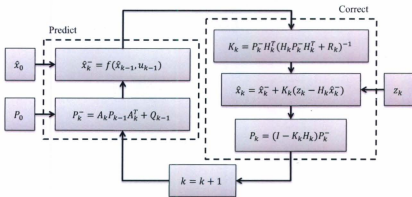


Figure 3.4: EKF block diagram.

The state vector, defined by Equation 3.29, is initialized with \hat{x}_0 which contains the starting attitude, heading, and bias estimates. The initial state covariance P_0 is also provided, and afterwards updated each calculation step. These are generally known in advance or a small initial value is assumed. Given the previous state and its covariance, the state covariance is updated using a linearization of the state transition function found using the Jacobian matrix and described in Section 3.3.1. The state prediction is then made with the state transition function f . In the correction step, the Kalman gain K_k is first calculated from the state and measurement covariances and the observation matrix H_k . The Kalman gain is then used to update the state to implement the EKF.

prediction with the error between the measurement and the current prediction. The state covariance is then again updated with information from the Kalman gain.

$$\hat{\mathbf{x}} := \begin{bmatrix} q_0 & q_1 & q_2 & q_3 & \mu_x & \mu_y & \mu_z \end{bmatrix}^T \quad (3.29)$$

The state vector contains the four quaternion elements, with q_0 being the scalar component, and the three gyroscope bias estimates. The input vector \mathbf{u}_k contains the corrected angular velocities, which are referred to explicitly in the following equations. Using the matrix form of the quaternion product in Equation 3.8, the state transition function is given by:

$$f(\hat{\mathbf{x}}_{k-1}, \mathbf{u}_{k-1}) = \begin{bmatrix} \begin{bmatrix} q_0 & -q_1 & -q_2 & -q_3 \\ q_1 & q_0 & -q_3 & q_2 \\ q_2 & q_3 & q_0 & -q_1 \\ q_3 & -q_2 & q_1 & q_0 \end{bmatrix} \begin{bmatrix} a_c \\ a_s \sigma_x \\ a_s \sigma_y \\ a_s \sigma_z \end{bmatrix} \\ \begin{bmatrix} \mu_x \\ \mu_y \\ \mu_z \end{bmatrix} \end{bmatrix} \quad (3.30)$$

where a_c and a_s are defined in equations 3.10 and 3.11, respectively, except:

$$\begin{bmatrix} \sigma_x & \sigma_y & \sigma_z \end{bmatrix}^T = \begin{bmatrix} (\omega_x - \mu_x) \Delta t & (\omega_y - \mu_y) \Delta t & (\omega_z - \mu_z) \Delta t \end{bmatrix}^T \quad (3.31)$$

and Δt is the calculation time-step. Therefore, the rate information with the estimated bias removed is integrated to predict the attitude and the gyroscope biases are modeled as constants.

The observation matrix, given by Equation 3.32, is linear in this case as the quaternion elements are provided directly by the measurement z_k .

$$H_k = \begin{bmatrix} 1 & 0 & 0 & 0 & 0 & 0 & 0 \\ 0 & 1 & 0 & 0 & 0 & 0 & 0 \\ 0 & 0 & 1 & 0 & 0 & 0 & 0 \\ 0 & 0 & 0 & 1 & 0 & 0 & 0 \\ 0 & 0 & 0 & 0 & 0 & 0 & 0 \\ 0 & 0 & 0 & 0 & 0 & 0 & 0 \\ 0 & 0 & 0 & 0 & 0 & 0 & 0 \end{bmatrix} \quad (3.32)$$

The only remaining requirements are the process and measurement covariances, Q_k and R_k , respectively. These depend on the sensor characteristics and are also used to tune the filter for performance for a given airframe and application. Tuning is not a major concern in this thesis as this is intended to be generally applied to a variety of platforms and only basic tuning was performed which involved characterizing the process noise Q_k from the sensor data sheets and then varying R_k to reduce attitude and gyroscope bias estimation error.

3.3 Original Contributions

The remaining sections of this chapter are original contributions developed for this particular application.

3.3.1 Jacobian calculation

The Jacobian matrix, defined here by Equation 3.33 is a matrix of partial derivatives of the state transition function with respect to each state variable. It is used to linearize the state transition function about the current state estimate and is also used in the update of the state error covariance as shown in Figure 3.4.

$$A_k := \frac{\partial f}{\partial \bar{\mathbf{x}}}_{\bar{\mathbf{x}}_{k-1}, \mathbf{u}_{k-1}} = \begin{bmatrix} \frac{\partial f_1}{\partial x_1} & \cdots & \frac{\partial f_1}{\partial x_7} \\ \vdots & \ddots & \vdots \\ \frac{\partial f_7}{\partial x_1} & \cdots & \frac{\partial f_7}{\partial x_7} \end{bmatrix}_{\bar{\mathbf{x}}_{k-1}, \mathbf{u}_{k-1}} \quad (3.33)$$

The gyroscope biases are present in all of the functions for the quaternion components, resulting in complex expressions for the partial derivatives of functions 1 ~ 4 with respect to states 5 ~ 7. Therefore, these expressions are given separately. The complete Jacobian matrix is then given by Equation 3.34.

$$A_k = \begin{bmatrix} a_c & -a_s \sigma_x & -a_s \sigma_y & -a_s \sigma_z & A_{1,5} & A_{1,6} & A_{1,7} \\ a_s \sigma_x & a_c & a_s \sigma_z & -a_s \sigma_y & A_{2,5} & A_{2,6} & A_{2,7} \\ a_s \sigma_y & -a_s \sigma_z & a_c & a_s \sigma_x & A_{3,5} & A_{3,6} & A_{3,7} \\ a_s \sigma_z & a_s \sigma_y & -a_s \sigma_x & a_c & A_{4,5} & A_{4,6} & A_{4,7} \\ 0 & 0 & 0 & 0 & 1 & 0 & 0 \\ 0 & 0 & 0 & 0 & 0 & 1 & 0 \\ 0 & 0 & 0 & 0 & 0 & 0 & 1 \end{bmatrix} \quad (3.34)$$

where

$$\begin{aligned} A_{1,5} &= \Delta t \left(q_1 a_s + q_0 \frac{a_s \sigma_x}{2} + \frac{(a_c - 2a_s)}{(2\sigma^2)} (q_1 \sigma_x \sigma_x + q_2 \sigma_x \sigma_y + q_3 \sigma_x \sigma_z) \right) \\ A_{1,6} &= \Delta t \left(q_2 a_s + q_0 \frac{a_s \sigma_x}{2} + \frac{(a_c - 2a_s)}{(2\sigma^2)} (q_1 \sigma_x \sigma_x + q_2 \sigma_x \sigma_y + q_3 \sigma_x \sigma_z) \right) \\ A_{1,7} &= \Delta t \left(q_3 a_s + q_0 \frac{a_s \sigma_x}{2} + \frac{(a_c - 2a_s)}{(2\sigma^2)} (q_1 \sigma_x \sigma_x + q_2 \sigma_x \sigma_y + q_3 \sigma_x \sigma_z) \right) \\ A_{2,5} &= \Delta t \left(-q_0 a_s + q_1 \frac{a_s \sigma_x}{2} + \frac{(a_c - 2a_s)}{(2\sigma^2)} (-q_0 \sigma_x \sigma_x + q_3 \sigma_x \sigma_y - q_2 \sigma_x \sigma_z) \right) \\ A_{2,6} &= \Delta t \left(q_3 a_s + q_1 \frac{a_s \sigma_x}{2} + \frac{(a_c - 2a_s)}{(2\sigma^2)} (-q_0 \sigma_x \sigma_x + q_3 \sigma_x \sigma_y - q_2 \sigma_x \sigma_z) \right) \\ A_{2,7} &= \Delta t \left(-q_2 a_s + q_1 \frac{a_s \sigma_x}{2} + \frac{(a_c - 2a_s)}{(2\sigma^2)} (-q_0 \sigma_x \sigma_x + q_3 \sigma_x \sigma_y - q_2 \sigma_x \sigma_z) \right) \end{aligned}$$

$$\begin{aligned}
A_{3,5} &= \Delta t \left(-q_3 a_s + q_2 \frac{a_s \sigma_x}{2} + \frac{(a_c - 2a_s)}{(2\sigma^2)} (-q_3 \sigma_x \sigma_x - q_0 \sigma_x \sigma_y + q_1 \sigma_x \sigma_z) \right) \\
A_{3,6} &= \Delta t \left(-q_0 a_s + q_2 \frac{a_s \sigma_x}{2} + \frac{(a_c - 2a_s)}{(2\sigma^2)} (-q_3 \sigma_x \sigma_x - q_0 \sigma_x \sigma_y + q_1 \sigma_x \sigma_z) \right) \\
A_{3,7} &= \Delta t \left(q_1 a_s + q_2 \frac{a_s \sigma_x}{2} + \frac{(a_c - 2a_s)}{(2\sigma^2)} (-q_3 \sigma_x \sigma_x - q_0 \sigma_x \sigma_y + q_1 \sigma_x \sigma_z) \right) \\
A_{4,5} &= \Delta t \left(q_2 a_s + q_3 \frac{a_s \sigma_x}{2} + \frac{(a_c - 2a_s)}{(2\sigma^2)} (q_2 \sigma_x \sigma_x - q_1 \sigma_x \sigma_y - q_0 \sigma_x \sigma_z) \right) \\
A_{4,6} &= \Delta t \left(-q_1 a_s + q_3 \frac{a_s \sigma_x}{2} + \frac{(a_c - 2a_s)}{(2\sigma^2)} (q_2 \sigma_x \sigma_x - q_1 \sigma_x \sigma_y - q_0 \sigma_x \sigma_z) \right) \\
A_{4,7} &= \Delta t \left(-q_0 a_s + q_3 \frac{a_s \sigma_x}{2} + \frac{(a_c - 2a_s)}{(2\sigma^2)} (q_2 \sigma_x \sigma_x - q_1 \sigma_x \sigma_y - q_0 \sigma_x \sigma_z) \right)
\end{aligned}$$

This expression for the Jacobian matrix was derived for this thesis. The derivation is not given here in the interest of brevity.

3.3.2 Logical constraints

Despite the elegance of the present mathematical framework, artifacts can occur in the attitude estimate under some circumstances. Inversion of the quaternion estimate is possible in two situations, which are described in the following subsections.

3.3.2.1 Gravity versus orientation

During level flight, the corrected gravity vector should not be positive, i.e. upward in the body frame of the aircraft. However, for example, during recovery of a dive, there can be a large upward acceleration, which can be greater than 1 g . The vector attitude calculation gives an independent estimate at each time-step, therefore during such a situation the attitude measurement will indicate inverted flight. A logical method to avoid attitude inversion is given by Algorithm 1.

```

// Get roll & pitch angles from latest quaternion estimate
roll = GetRoll(Q);
pitch = GetPitch(Q);
if |roll| < 90° and |pitch| < 90° then           // If upright
    if az > 0 then                             // If gravity upward
        | skip measurement;
    end
else                                           // If inverted
    if az < 0 then                             // If gravity downward
        | skip measurement;
    end
end

```

Algorithm 1: Inverted gravity correction.

Therefore, if the aircraft is within 90° in roll or pitch, the gravity estimate should never be upward. If the sensors indicate that it is, then the measurement will be excluded and gyroscope angular rates are used to predict the attitude. Conversely, if the aircraft is beyond 90° in roll or pitch, then the gravity estimate should not be downward in the body frame. An example of the result when this is not used is shown at the end of Section 4.1.1.1.

3.3.2.2 Quaternion continuity

As mentioned in Section 3.2.2.2, the overall sign of the quaternion from the vector attitude measurement is irrelevant to the solution of the proper rotation matrix. The attitude is calculated at each time-step with new sensor information and is therefore independent of previous measurements. The filtered attitude estimate, however, requires continuity of the measurement and estimate for accuracy. In some orientations, the attitude measurement will change overall sign. Inversion of the quaternion attitude measurement is detected and the sign is corrected by Algorithm 2.

```
if  $|\hat{Q}_k - \hat{Q}_{k-1}| > 1$  then // Quaternion modulus
|  $\hat{Q}_k = -\hat{Q}_k$ 
end
```

Algorithm 2: Correction for quaternion inversion.

If the difference between the current attitude measurement and the previous filtered attitude estimate is greater than 1, then the overall sign of the new attitude measurement is reversed. The quaternion of rotation has magnitude 1 by definition and therefore a difference greater than this value indicates a complete rotation in a single time-step, which is not possible for an aircraft. An example of the result when this is not used is shown at the end of Section 4.1.1.3.

This concludes the mathematical details of the AHRS algorithm: the quaternion angular rate integration, vector attitude measurement including centripetal and model-based acceleration correction, EKF and derivation of the Jacobian matrix, and logical constraints. The following chapter describes the results of simulation which illustrate some of the effects of the acceleration correction and logical constraints, and results from a flight test.

Chapter 4

Simulation & Experimental Results

This chapter is divided into two sections: results from simulation and flight test results. Simulation comprises the most significant portion of the results as this was the method used to develop and validate the AHRS algorithm developed in the previous chapter. The flight test is based on an actual flight conducted in the field by the RAVEN team. The details of these are presented in the following sections.

4.1 Simulation

The AHRS was validated in simulation, mainly using MATLAB. Simulation is necessary for development because the true values of the attitude and heading can be obtained for validation, which can be difficult to do for field trials. The simulation also provides the necessary measurement values for the AHRS including body-frame acceleration and angular velocity, airspeed, and elevator input. Magnetometer outputs in three dimensions are generated using the true orientation based on a given reference unit vector for north as in Equation 4.1:

$$\mathbf{m}^b = C^{-1}\mathbf{m}^n \quad (4.1)$$

where C is a rotation matrix representation of the true attitude.

The inertial measurements are simulated using a noise model typical of MEMS accelerometers and gyroscopes given by Equations 4.2 and 4.3:

$$\tilde{h} = h + \mu_h + v \quad (4.2)$$

and

$$\dot{\mu}_h = \mu_h + w \quad (4.3)$$

where v and w are Gaussian white-noise processes, \tilde{h} represents one channel of measurement, h is the true value, and μ_h is the bias.

The variances for the initial bias, in-run bias stability, and output noise are taken from the data sheet for the ADIS16364 IMU [43] and given in terms of standard deviations in Table 4.1.

Sensor	Characteristic	Value ($\pm 1\sigma$)	Units
Gyroscope	initial bias	3	$^{\circ}/\text{sec}$
	in-run bias stability	0.007	$^{\circ}/\text{sec}$
	output noise	0.8	$^{\circ}/\text{sec}$
Accelerometer	initial bias	8	mg
	in-run bias stability	0.1	mg
	output noise	5	mg

Table 4.1: ADIS16364 noise characteristics for simulation.

The magnetometer outputs each have Gaussian white-noise added with a variance of 0.01, unit-less because the magnetic reading was generated from a normalized reference. Likewise, the airspeed has white-noise added with a variance of 6.25. These noise figures were chosen based on experience and are substantially higher than those applied to the inertial sensors to represent the disturbances inherent in magnetic and airspeed measurements which have unmodeled disturbance effects. While specific

quantities from this particular sensor package were used, the AHRS algorithm is intended to be used with any sensor package with little tuning.

4.1.1 MATLAB Simulation

The MATLAB simulation was based on Airlib, which is a Simulink aircraft model library created by Campa [44]. The model used is based on the IAI Pioneer airframe. A simple PID-based controller was designed to control the model in terms of roll angle, airspeed, altitude, and sideslip angle.

Simulation runs were performed to verify the performance of the AHRS algorithm in terms of both attitude and bias estimation error. The errors for many AHRS occur during constant banked turns and high- g maneuvers. The simulation scenarios are designed to evaluate these situations with increasing complexity. They are all based on 100 seconds of simulation with variations in the input to the flight controller. However, the trajectory of the aircraft is not controlled; only the roll angle, airspeed, altitude, and sideslip angle are controlled. Therefore, the resulting attitude, heading, and trajectory response is due to the controller and can vary significantly between scenarios with only subtle input changes. This is partly irrelevant because the desired maneuvers are still achieved, with the main interest being the banked turn and high- g turns. A brief summary of each simulation run is listed here:

- Run A begins with level flight moving into a banked turn at 45° to the right and held for almost a complete (360°) rotation of heading then smoothly transitioned to a banked turn at 45° to the left, which is held for another complete rotation of heading then returned to level flight.
- Run B is the same as Run A only the transition time between the two banked turns is significantly reduced. This results in a sharp reversal of heading repre-

sentative of a CA maneuver.

- Run C is the same as Run B with an airspeed increase during the transition between banked turns. The result is another sharp reversal of heading at a higher airspeed which can be considered a high- g maneuver.

To estimate the vertical acceleration from the elevator input as described in Section 3.2.2.4, system identification techniques were used on a separate simulation similar to those described but with different banked turn angles to prevent the effect of fitting the data. The model identified is used as part of the AHRS in all of the following simulations unless otherwise noted. The results of the system identification are described in Section 4.1.1.4.

The specific attitude and trajectory of each of the simulations is given in the following subsections along with the results. The trajectory plots were generated using the script by Scordamaglia [45]. Due to MATLAB limitations, the reference system is not consistent with Figure 3.2, but the visualization effect is the same. The airframe 3D model is not representative of the simulated aircraft.

4.1.1.1 Run A: smooth turns

The first simulation scenario was chosen to demonstrate attitude and heading estimating during banked turns without large acceleration disturbances. The control reference inputs are given by Table 4.2.

The reference is linearly interpolated between each time specification which allows control over the reference rate of change. In this simulation, 10 seconds were given between the banked turn reversal.

A 3D perspective of the attitude and trajectory is shown in Figure 4.1. The corresponding plot of attitude angles is given directly below in Figure 4.2. The heading

Time (sec)	Roll Angle ($^{\circ}$)	Altitude (m)	Speed (m/sec)
0	0	100	60
20	0	100	60
25	-45	100	60
45	-45	100	60
55	45	100	60
75	45	100	60
80	0	100	60
100	0	100	60

Table 4.2: MATLAB simulation run A input parameters.

is wrapped about $\pm 180^{\circ}$ in all attitude angle plots for consistency.

The estimation error is very small and it is difficult to discern the estimate from the true attitude in the attitude plot. The error between the estimate and the true attitude is shown more clearly in Figure 4.3.

The bias estimation with the true randomly generated bias and the EKF estimate is shown in Figure 4.4. In each axis, the bias estimate tracks the true value well, with a good estimate being obtained after about 40 seconds of simulation. The initial bias is assumed to be zero for all axes, in practice, a better initial estimate could be provided with calibration. However, the worst case scenario of assuming zero knowledge of the bias is used to demonstrate the EKF performance.

Referring to Figures 4.3 and 4.4 simultaneously, it can be seen that the error is significantly reduced once a good estimate of the gyroscope bias is obtained. This is true because the two banked turn maneuvers are very similar, so the only difference between the left (second) turn and the right turn is the better bias estimate, resulting in a smaller error.

The gyroscope bias is randomly generated using the specifications in Table 4.1, and is therefore different in each simulation run. To evaluate the performance of the EKF on average, several runs were performed to obtain a Root Mean Square (RMS)

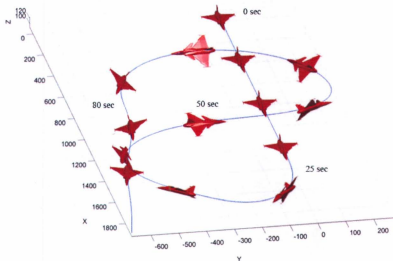


Figure 4.1: 3D perspective of attitude and trajectory for run A with approximate time labels indicated.

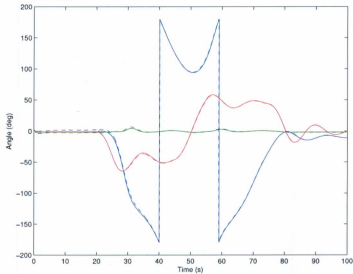


Figure 4.2: True (solid) and estimated (dashed) attitude angles for run A. Yaw, pitch, and roll are blue, green, and red, respectively.

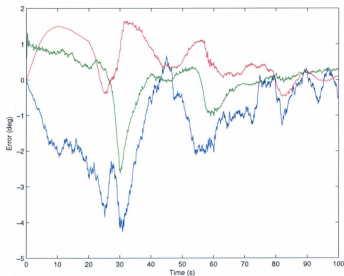


Figure 4.3: Attitude estimate error for run A. Yaw, pitch, and roll error are blue, green, and red, respectively.

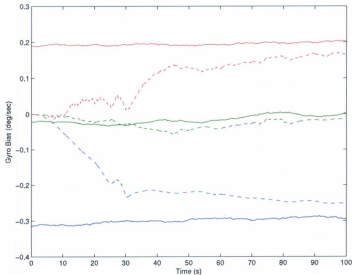


Figure 4.4: True (solid) and estimated (dashed) gyro biases for run A. X, Y, and Z gyroscope biases are blue, green, and red, respectively.

RMS Error	Yaw	Pitch	Roll	Units
Attitude Angle	2.02 \pm 2.13	1.46 \pm 1.56	1.29 \pm 1.01	$^{\circ} \pm 1\sigma$
Gyroscope Bias	0.15 \pm 0.19	0.19 \pm 0.22	0.14 \pm 0.14	$^{\circ}/\text{sec} \pm 1\sigma$

Table 4.3: MATLAB simulation run A error figures (10 runs).

error for each run. This RMS error was averaged over 10 runs. The average RMS error and standard deviation is given in Table 4.3.

In this scenario, the greatest error is in yaw, and the smallest error in roll. Generally, there is less heading information available than roll and pitch, particularly during a smooth flight. This is because the gravity measurement provides no heading information and the magnetic field is subject to disturbances, which are modeled here with higher noise figures. Roll and pitch have more correction data available from the gravity measurement and during smooth flight can produce a good estimate.

Figure 4.5 shows the roll angle estimate versus the true roll angle when no gravity logic correction is used. The acceleration becomes inverted in the vertical axis, resulting in an inverted attitude which causes a discontinuity in the EKF estimate that returns to the true value after some time.

4.1.1.2 Run B: turns with sharp transition

The second simulation scenario is based on the previous simulation with the only change being the duration of the transition between the two banked turns. Due to the controller, this results in a sharp U-turn which is representative of a CA maneuver. The simulation input parameters are given in Table 4.4.

Instead of interpolating for 10 seconds between the right banked turn and the left, the interpolation is performed within 2 seconds. All other simulation parameters remain the same.

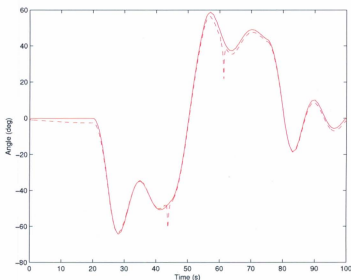


Figure 4.5: True (solid) and estimated (dashed) roll angles for run A without gravity logic correction. The discontinuities are caused by vertical gravity inversions.

Time (sec)	Roll Angle ($^{\circ}$)	Altitude (m)	Speed (m/sec)
0	0	100	60
20	0	100	60
25	-45	100	60
49	-45	100	60
51	45	100	60
75	45	100	60
80	0	100	60
100	0	100	60

Table 4.4: MATLAB simulation run B input parameters.

The 3D perspective of the attitude and trajectory is shown in Figure 4.6. The time plot of the attitude angles is given in Figure 4.7.

From the trajectory plot, the sharp turn can be seen around the 50 second mark. The error is greatest at this point due to the acceleration disturbances. From Figure

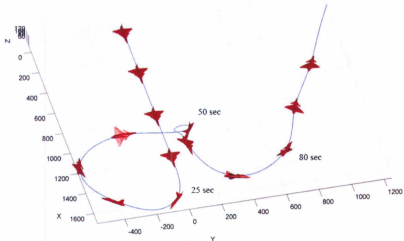


Figure 4.6: 3D perspective of attitude and trajectory for run B with approximate time labels indicated.

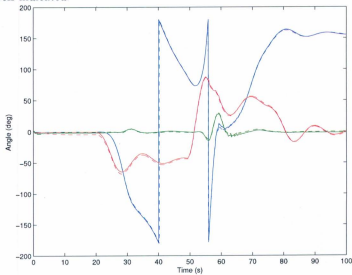


Figure 4.7: True (solid) and estimated (dashed) attitude angles for run B. Yaw, pitch, and roll are blue, green, and red, respectively.

4.8 it is seen that the error grows initially as the gyroscope biases are determined, then the error sharply grows during the transition between the two banked turns. The error is then reduced as the trajectory steadies and the gyroscope biases are determined. The gyroscope bias estimation can be seen in Figure 4.9.

This simulation was also performed 10 times with randomly generated gyroscope biases and measurement noise. The average RMS errors and their standard deviations for the angles and gyroscope biases is given in Table 4.5.

RMS Error	Yaw	Pitch	Roll	Units
Attitude Angle	1.76 \pm 1.59	1.66 \pm 1.24	1.72 \pm 1.56	$^{\circ} \pm 1\sigma$
Gyroscope Bias	0.13 \pm 0.13	0.20 \pm 0.19	0.17 \pm 0.20	$^{\circ}/\text{sec} \pm 1\sigma$

Table 4.5: MATLAB simulation run B error figures (10 runs).

Overall, the attitude error is on average higher than the previous simulation scenario, as is expected. However, the heading error is slightly reduced which may be due to the increased amount of data available as the heading changes.

The results are good as the error remains very low for this scenario which demonstrates a sharp maneuver applicable to CA.

The effect of acceleration correction is clear in Figure 4.10. Pure gravitational acceleration measurement will never exceed 1 g in total magnitude, by definition, but in this simulation, uncorrected accelerations exceed 8 g . This demonstrates the overwhelming effect of non-gravitational acceleration disturbances. Also from the figure, it can be seen that Y-axis acceleration is close to zero without correction during the banked turns. This is due to the centripetal acceleration which negates the component of gravity present in the Y-axis measurement during the 45 degree banked turns.

As stated in the introduction, the work by Beaudette [1] indicates that human

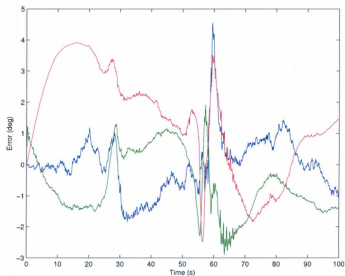


Figure 4.8: Attitude estimate error for run B. Yaw, pitch, and roll error are blue, green, and red, respectively.

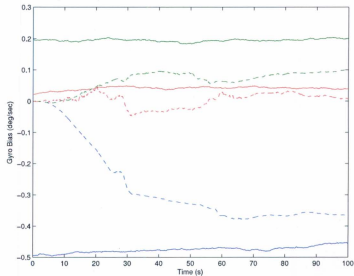


Figure 4.9: True (solid) and estimated (dashed) gyro biases for run B. X, Y, and Z gyroscope biases are blue, green, and red, respectively.

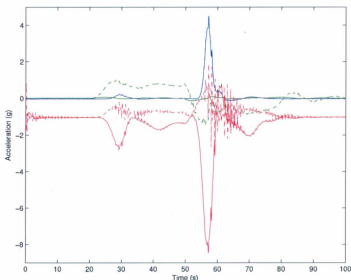


Figure 4.10: Non-corrected (solid) and corrected (dashed) accelerations for run B. X, Y, and Z axes are blue, green, and red, respectively.

pilots can become unconscious with accelerations greater than $5 g$. In this simulation, accelerations were greater than $8 g$. The AHRS is still able to track the attitude with reasonable accuracy during this time which demonstrates that unmanned aircraft are certainly capable of more extreme maneuvers than manned aircraft.

4.1.1.3 Run C: turns with sharp transition and airspeed increase

The third scenario is an extension of the previous simulation with an airspeed increase during the transition between banked turns. The airspeed is increased by 20 m/sec as shown in Table 4.6.

By increasing the airspeed during the banked turn transition, the non-gravitational accelerations experienced are also increased. Therefore, this scenario is indicative of a high- g maneuver.

Time (sec)	Roll Angle ($^{\circ}$)	Altitude (m)	Speed (m/sec)
0	0	100	60
20	0	100	60
25	-45	100	60
49	-45	100	80
51	45	100	80
75	45	100	60
80	0	100	60
100	0	100	60

Table 4.6: MATLAB simulation run C input parameters.

The 3D perspective of the attitude and trajectory is shown in Figure 4.11. Despite the subtle change in airspeed only from the previous scenario, the trajectory is significantly changed. This is due in part to the controller used to control the simulation. The result, however, is the sharp banked turn near the 50 second mark. The attitude plot is shown in Figure 4.12.

The attitude plot shows that the estimation error is greater than in the previous simulations, particularly near the 50 second mark. The error is shown in more detail in Figure 4.13. As with the other simulations, the error grows initially with an inaccurate bias estimate, then becomes more accurate as the true bias is found. The large error spike during the sharp turn is due to the large non-gravitational accelerations experienced by taking this turn at a higher airspeed. Once the trajectory has returned to steady flight the error is significantly reduced and the bias estimate is good as shown in Figure 4.14.

This simulation scenario has consistently larger errors than either of the previous simulations. The average RMS error for attitude angle and gyroscope bias with their standard deviations is given in Table 4.7.

The average attitude angle error is greater than in any of the previous simulations. The error remains small, despite this, and the results show that estimating even during

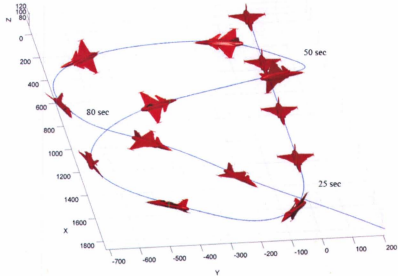


Figure 4.11: 3D perspective of attitude and trajectory for run C with approximate time labels indicated.

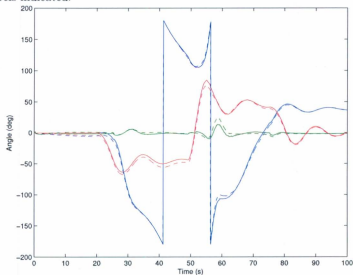


Figure 4.12: True (solid) and estimated (dashed) attitude angles for run C. Yaw, pitch, and roll are blue, green, and red, respectively.

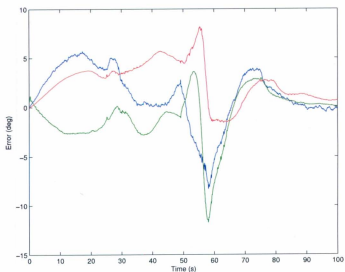


Figure 4.13: Attitude estimate error for run C. Yaw, pitch, and roll error are blue, green, and red, respectively.

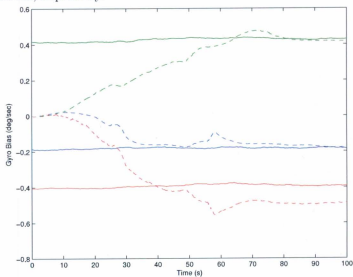


Figure 4.14: True (solid) and estimated (dashed) gyro biases for run C. X, Y, and Z gyroscope biases are blue, green, and red, respectively.

RMS Error	Yaw	Pitch	Roll	Units
Attitude Angle	2.80 ± 1.99	3.08 ± 1.35	2.67 ± 1.45	$^{\circ} \pm 1\sigma$
Gyroscope Bias	0.21 ± 0.18	0.18 ± 0.18	0.16 ± 0.16	$^{\circ}/\text{sec} \pm 1\sigma$

Table 4.7: MATLAB simulation run C error figures (10 runs).

high- g maneuvers can be moderately accurate.

Figure 4.15 shows the attitude angle estimates versus the true attitude angles when no quaternion inversion logic correction is used. The quaternion attitude becomes inverted, but still represents the same overall attitude. However, the EKF cannot handle these discontinuities and large errors occur as a result.

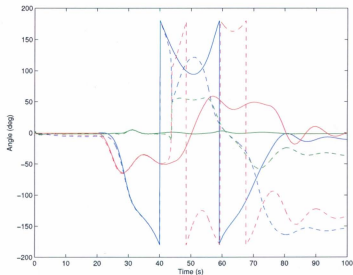


Figure 4.15: True (solid) and estimated (dashed) attitude angles for run C without quaternion inversion correction. Yaw, pitch, and roll are blue, green, and red, respectively.

4.1.1.4 System identification of model parameters

The total acceleration experienced by the aircraft is due to the sum of gravity, centripetal acceleration, and translational acceleration. As discussed in Section 3.2.2.4, it is possible to estimate the vertical component of the translational acceleration from the elevator input under standard flight conditions (i.e. no strong wind disturbance or stall condition). Statistical system identification techniques were used to identify such a model for acceleration correction in this simulation. The identification data including the elevator input scaled by squared airspeed, the input, and the Z-axis acceleration with centripetal acceleration and gravity removed, the output, are shown in Figure 4.16.

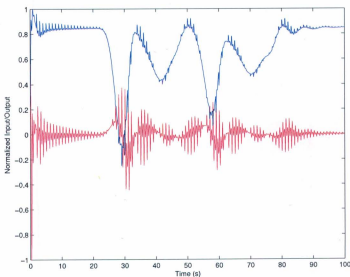


Figure 4.16: Elevator input (blue) and Z-axis vertical acceleration with centripetal acceleration and gravity removed (red). Both are normalized.

The system was identified in this case using the N4SID algorithm¹ described by Ljung [41]. This is a state-space identification technique and the model order was chosen as 2, from analysis of the results with various orders. The resulting state-space model, in this case, is given by Equation 4.4.

$$\begin{aligned} \begin{bmatrix} x_{1,k+1} \\ x_{2,k+1} \end{bmatrix} &= \begin{bmatrix} 0.7839 & -0.5784 \\ 0.1766 & 0.5562 \end{bmatrix} \begin{bmatrix} x_{1,t} \\ x_{2,t} \end{bmatrix} + 1.0^{-3} \begin{bmatrix} -0.2884 \\ -0.1645 \end{bmatrix} \delta_c v_a^2 \\ a_{t,z} &= \begin{bmatrix} 18.6362 & -7.1273 \end{bmatrix} \begin{bmatrix} x_{1,t} \\ x_{2,t} \end{bmatrix} \end{aligned} \quad (4.4)$$

with the initial condition $x_{1,0}, x_{2,0} = -0.0877, -0.2286$. This initial condition is required for these simulations as they begin in flight, but may be zero for a flight beginning on the ground. These states and parameters have no physical meaning and are a result of the chosen model order. This model is a statistical fit based on the relationship in Equation 3.28 and therefore has no algebraic derivation.

The result of this model is shown in Figure 4.17. The results show a good correspondence between the model output and the original acceleration.

Using the model for correction is more effective when the acceleration disturbance is high. For example, the error results are not significantly different for simulation run A without model correction. The error for simulation run B, however, is consistently greater without model correction. A comparison of the error results is shown in Table 4.8.

The attitude plot for simulation run B without model-based correction is shown in

¹This simulation was conducted with a closed loop controller. The N4SID algorithm does not account for correlation between the input and output from controller behavior. However, the system identification result is accurate for the open loop identification method. Identification of the model from flight test data will generally be from manually piloted flight and therefore can be assumed uncorrelated because the pilot response is not as direct as an automatic controller.

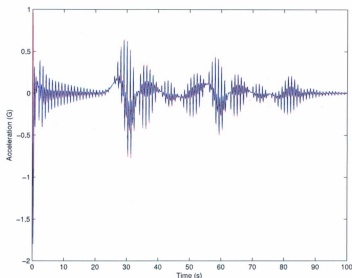


Figure 4.17: System identification results showing model estimate (blue) of Z-axis vertical acceleration without centripetal acceleration and gravity (red) from elevator input data.

RMS Error	Yaw	Pitch	Roll	Units
Run A with model	2.02 ± 2.13	1.46 ± 1.56	1.29 ± 1.01	$^{\circ} \pm 1\sigma$
Run A without model	2.59 ± 3.13	1.06 ± 1.10	1.33 ± 1.61	$^{\circ} \pm 1\sigma$
Run B with model	1.76 ± 1.59	1.66 ± 1.24	1.72 ± 1.56	$^{\circ} \pm 1\sigma$
Run B without model	2.40 ± 2.28	1.77 ± 1.65	1.95 ± 1.29	$^{\circ} \pm 1\sigma$

Table 4.8: Error comparison for simulation runs A and B with and without model correction (10 runs).

Figure 4.18. This plot shows notably more error than Figure 4.7, particularly during the transition between turns at 50 seconds.

Identification of the model for a specific airframe requires a controlled flight test with a truth measurement of attitude, from a non-inertial source. The correct gravity vector can then be determined and removed from the total acceleration measurement

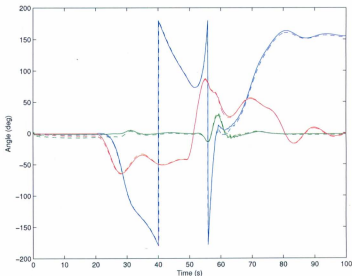


Figure 4.18: True (solid) and estimated (dashed) attitude angles for run B without model-based correction. Yaw, pitch, and roll are blue, green, and red, respectively.

along with the calculated centripetal acceleration. The elevator input and airspeed are recorded for the input and the remaining acceleration is used as the output for the system identification.

4.1.1.5 Centripetal acceleration correction

The most significant component of non-gravitational acceleration disturbance is from centripetal acceleration effects. Removal of these accelerations from the measurement is a major requirement of an AHRS for CA. To demonstrate the necessity of this correction, several simulation runs were conducted without centripetal or model correction based on the above scenarios for comparison.

The non-corrected results for run A are shown in Figure 4.19. The estimation error during the banked turns and transition is much higher than the error when

correction is used. The estimated pitch angle is particularly misleading as it should be much closer to zero than is estimated. The roll and heading angles, while still exhibiting error, are not as severely misleading and may not greatly affect the control of the aircraft.

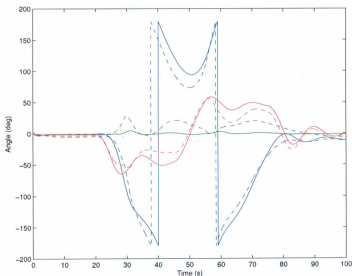


Figure 4.19: True (solid) and estimated (dashed) attitude angles for run A without centripetal or model-based correction. Yaw, pitch, and roll are blue, green, and red, respectively.

The non-corrected results for run B are shown in Figure 4.20. The estimation error is even larger in this case as the sharp transition between banked turns results in a larger acceleration disturbance. The 55 second mark shows that the estimation error is high for both roll and heading, which could result in incorrect control of the aircraft.

The AHRS algorithm was evaluated without acceleration correction for 10 runs as with the previous scenarios for comparison. The results are shown in Table 4.9.

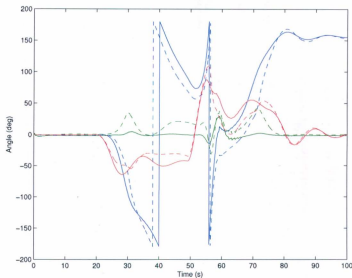


Figure 4.20: True (solid) and estimated (dashed) attitude angles for run B without centripetal or model-based correction. Yaw, pitch, and roll are blue, green, and red, respectively.

RMS Error	Yaw	Pitch	Roll	Units
Run A with correction	2.02 ± 2.13	1.46 ± 1.56	1.29 ± 1.01	$^\circ \pm 1\sigma$
Run A without correction	12.63 ± 2.04	10.43 ± 2.07	9.86 ± 2.83	$^\circ \pm 1\sigma$
Run B with correction	1.76 ± 1.59	1.66 ± 1.24	1.72 ± 1.56	$^\circ \pm 1\sigma$
Run B without correction	20.06 ± 5.55	12.69 ± 3.92	11.67 ± 2.16	$^\circ \pm 1\sigma$

Table 4.9: Error comparison for simulation runs A and B with and without centripetal and model-based correction (10 runs).

These results show that the average RMS error for all angles is nearly an order of magnitude higher when non-corrected versus corrected even for the smooth turn case of run A. For run B with the fast transition between the two banked turns, the average RMS error is noticeably higher than the previous case. This supports the use of the approximation described in Section 3.2.2.3 for the centripetal acceleration estimate

used to correct the acceleration measurement.

4.2 Flight Test

The AHRS was also evaluated with data from a live test flight. The test flight included both manual and autopilot controlled flight using the MicroPilot [46] autopilot. This autopilot is also based on inertial sensors and therefore cannot be considered a true measurement for attitude and heading. However, a comparison can still be made between the AHRS performance in this thesis versus the MicroPilot reported attitude. The flight test was conducted in Argentia, NL with a Giant Big Stik airframe.

The estimated attitude versus the MicroPilot data is shown in Figure 4.21. This plot shows only a segment of the flight for clarity, but is typical of the entire flight. There is no 3D perspective of the attitude and trajectory in this case due to lack of position data, but interpretation of the attitude plot can show that a rectangular flight path is being followed with some wind. For example, from 25 to 40 seconds the aircraft is in steady flight against the wind then from 40 to 48 seconds reverses direction, travels downwind, and from 51 to 56 seconds reverses direction again to complete the path. These times are approximate.

The error is shown in more detail in Figure 4.22. These errors are large at times, reaching $\pm 30^\circ$. However, it can be observed that much of the error is somewhat constant, at least for each segment of the flight. This may be due to calibration or misalignment which is internally corrected in the MicroPilot. For example, the average pitch angle shows an offset error of about 5 degrees. The error spikes occur during the turning maneuvers which may result from gyroscope scale calibration, also internally corrected, or wind disturbance.

The overall error figures are given in Table 4.10. A standard deviation is given

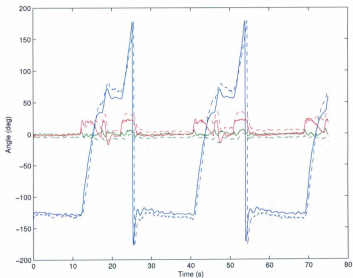


Figure 4.21: MicroPilot (solid) and estimated (dashed) attitude angles for field test. Yaw, pitch, and roll are blue, green, and red, respectively.

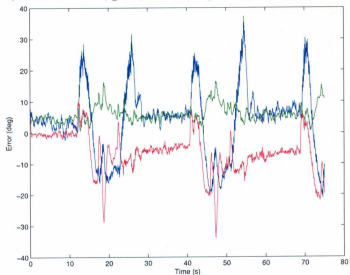


Figure 4.22: Attitude estimate error for field test. Yaw, pitch, and roll error are blue, green, and red, respectively.

RMS Error	Yaw	Pitch	Roll	Units
Attitude Angle	11.7 ± 2.27	6.52 ± 0.69	8.82 ± 0.96	$^{\circ} \pm 1\sigma$

Table 4.10: Error between AHRS and MicroPilot reported attitude (10 runs).

which is due to the generation of the magnetic measurement which was not available from the MicroPilot data, and therefore had random noise added as with the simulation. The average RMS error of the estimation versus MicroPilot reported attitude is acceptable, particularly the lower roll and pitch error. The true attitude is not known, therefore it is not possible to say whether this error is a fault of either AHRS solution as there is no information available to indicate the extent of MicroPilot reported attitude error during banked turns.

Chapter 5

Conclusion

5.1 Summary

The development of an AHRS to fulfill the sensor requirement for CA with sUA is described in the previous chapters. The requirement in this case was determined to be an AHRS that gives an accurate estimate of attitude and heading for any aircraft orientation and under high- g motion conditions.

The technical difficulties present in this task included mitigating gyroscope bias integration error, gravity measurement obscuration by non-gravitational accelerations, magnetic field distortions affecting compass measurement, and resolving the gyroscope and vector attitude measurements into a common, unique attitude representation.

The gyroscope bias integration error was corrected by integration of many existing techniques. A non-linear filtering solution, the EKF, was used to filter the attitude estimate from the gyroscope integration using vector attitude measurements while tracking the gyroscope biases. This is a standard technique that has been successfully applied many times, and the results in this thesis show good performance in bias estimation.

The vector measurement is dependent on a reliable measurement of gravity, but this is commonly obscured by non-gravitational accelerations. To overcome this, non-gravitational accelerations are estimated and removed from the measurement. It is shown that centripetal acceleration approximation, as used by some other authors, can significantly improve the gravity measurement. Model-based estimation, also used by others, of the non-gravitational acceleration is also applied and improves the accuracy of the attitude estimate during high- g maneuvers.

The magnetic field distortion is not addressed in detail. The magnetometer measurements were generated for both the simulations and the flight test as they were unavailable in each. A large noise figure was used to add noise to represent the distortions which were not easily modeled. Also, the vector attitude measurement utilized has an allowance for weighting each vector, i.e. magnetic versus gravity.

Finally, resolving the gyroscope and vector attitude measurements into a common attitude representation presents some difficulty. While the quaternion representation was used for each, the gyroscope attitude is the result of integration and the vector attitude is calculated at each time step. To preserve the continuity of the vector attitude estimate, two logical constraints developed for this thesis were applied which showed good results in maintaining a smooth estimate.

It is not known whether CA can be successfully accomplished with existing AHRS solutions. The sensor requirement is not yet defined by any authority. It is unlikely that current MEMS-based systems will perform sufficiently for control during extreme maneuvers. Therefore, focus on the development of an AHRS that gives a robust estimate during CA maneuvers could improve the safety of all aircraft by allowing better avoidance control. The results are positive in obtaining an accurate attitude estimate during CA maneuvers for sUA.

5.1.1 Contributions

The quaternion-based EKF is chosen as the filtering solution and attitude representation. The EKF requires a Jacobian matrix of partial derivatives of the state transition function with respect to the state variables. The state vector contains the gyroscope biases and, as a result, the Jacobian matrix contains some lengthy expressions. The analytic expression of the Jacobian matrix for a quaternion-based EKF including gyroscope biases is given as an original contribution.

Centripetal acceleration correction is rarely mentioned in the academic literature for AHRS, but is indispensable for accurate attitude estimation during banked turns. An approximation as used in Euston et al. [7] is used to estimate the centripetal acceleration. While other sources also consider centripetal acceleration correction, it is essential to high performance AHRS, as demonstrated in Section 4.1.1.5. Aiding of inertial navigation systems (INS) by vehicle dynamics modeling is not unique and has been covered, for example, by Hegrenaes et al. [25] and Koifman and Bar-Itzhack [24]. However, the practical application of vehicle model information to aid an AHRS is still uncommon, and is shown to offer significant improvement for high- g maneuvers.

In this thesis, these methods are combined to create an AHRS that performs well during extreme maneuvers representative of CA. All elements required for software implementation are given in the previous chapters. Simulation results are used to validate the AHRS and demonstrate the performance of acceleration correction. Flight test data is used for further validation versus existing sensor systems. The main contribution is the design of a new attitude sensing solution that can improve high- g maneuvers using existing autopilot hardware.

5.2 Future Work

The field-conducted flight test data used was not specifically designed for this thesis. Therefore, CA maneuvers are not performed nor is the proper data or quality of data recorded for AHRS development. A flight test with CA maneuvers and an independent measurement of attitude is required to confirm the AHRS results. The other sensors required for such a flight test are an IMU with triaxial accelerometers and gyroscopes, triaxial magnetometers, airspeed, aircraft control inputs, and preferably GPS data. The independent attitude could be obtained via horizon tracking with a camera.

The aircraft model used in this thesis is a simple linearized model. With the modern availability of powerful processors, a more complex model could be used to estimate the acceleration in a number of axes for measurement correction, or even estimate other parameters such as angular velocity. On-line system identification could be used to estimate the model parameters during flight, allowing for the system to be more readily adapted to new platforms. Wind modeling should be included as a correction term for the vector attitude measurement and the effect of wind on the attitude should be quantified.

The next step after an AHRS for CA has been developed is the extension to automatic control. With a proper controller, the AHRS could be revised to provide improved feedback for CA.

Finally, the real-time implementation of this algorithm remains. The computational burden is not an issue as the algorithm is much faster than real-time even when running in MATLAB without optimization on a mid-performance PC.

Bibliography

- [1] D. Beaudette, "A hazard in aerobatics: effects of G-forces on pilots." *Federal Aviation Administration*, no. 91-61, 1984.
- [2] W. Harman, "TCAS: a system for preventing midair collisions," *The Lincoln Laboratory Journal*, vol. 2, pp. 437-458, 1989.
- [3] "FLARM Technology," 2010. [Online]. Available: <http://www.flarm.com/>
- [4] R. Van Gent, J. Hoekstra, and R. Ruigrok, "Free flight with airborne separation assurance," in *Proc. CEAS symposium*, 1997.
- [5] M. Shuster, "A survey of attitude representations," *Navigation*, vol. 8, p. 9, 1993.
- [6] R. Mahony, T. Hamel, and J. M. Pfimlin, "Nonlinear complementary filters on the special orthogonal group," *Automatic Control, IEEE Transactions on*, vol. 53, no. 5, pp. 1203-1218, june 2008.
- [7] M. Euston, P. Coote, R. Mahony, J. Kim, and T. Hamel, "A complementary filter for attitude estimation of a fixed-wing uav," in *Intelligent Robots and Systems, 2008. IROS 2008. IEEE/RSJ International Conference on*, sept. 2008, pp. 340-345.
- [8] E. Edwan, J. Zhang, J. Zhou, and O. Loffeld, "Reduced DCM based attitude estimation using low-cost IMU and magnetometer triad," in *Positioning Navi-*

- gation and Communication (WPNC), 2011 8th Workshop on, april 2011, pp. 1-6.
- [9] J. Wertz, *Spacecraft attitude determination and control*. Kluwer Academic Pub, 1978, vol. 73.
- [10] S. Altmann, "Hamilton, Rodrigues, and the quaternion scandal," *Mathematics Magazine*, vol. 62, no. 5, pp. 291-308, 1989.
- [11] I. Bar-Itzhack and Y. Oshman, "Attitude determination from vector observations: Quaternion estimation," *Aerospace and Electronic Systems, IEEE Transactions on*, vol. AES-21, no. 1, pp. 128-136, jan. 1985.
- [12] D. Choukroun, I. Bar-Itzhack, and Y. Oshman, "Novel quaternion Kalman filter," *Aerospace and Electronic Systems, IEEE Transactions on*, vol. 42, no. 1, pp. 174-190, jan. 2006.
- [13] J. Hall, N. Knoebel, and T. McLain, "Quaternion attitude estimation for miniature air vehicles using a multiplicative extended Kalman filter," in *Position, Location and Navigation Symposium, 2008 IEEE/ION*. IEEE, 2008, pp. 1230-1237.
- [14] J. Marins, X. Yun, E. Bachmann, R. McGhee, and M. Zyda, "An extended Kalman filter for quaternion-based orientation estimation using MARG sensors," in *Intelligent Robots and Systems, 2001. Proceedings. 2001 IEEE/RSJ International Conference on*, vol. 4. Ieee, 2001, pp. 2003-2011.
- [15] D. Titterton and J. Weston, *Strapdown inertial navigation technology*, 2nd ed. The Institution of Electrical Engineers, 2004.

- [16] R. Kalman, "A new approach to linear filtering and prediction problems," *Journal of basic Engineering*, vol. 82, no. Series D, pp. 35-45, 1960.
- [17] J. L. Crassidis, F. L. Markley, and Y. Cheng, "Nonlinear attitude filtering methods," in *J. Guidance, Control, Dynam.*, vol. 30, no. 1, jan. 2007, pp. 12-28.
- [18] J. Murrell, "Precision attitude determination for multimission spacecraft," in *Guidance and Control Conference*, vol. 1, 1978, pp. 70-87.
- [19] M. Shuster and S. Oh, "Three-axis attitude determination from vector observations," *Journal of Guidance and Control*, vol. 4, pp. 70-77, 1981.
- [20] M. Shuster, "A simple Kalman filter and smoother for spacecraft attitude," *Journal of the Astronautical Sciences*, vol. 37, no. 1, pp. 89-106, 1989.
- [21] S. Pourtakdoust and H. Asl, "An adaptive unscented Kalman filter for quaternion-based orientation estimation in low-cost AHRS," *Aircraft Engineering and Aerospace Technology: An International Journal*, vol. 79, no. 5, pp. 485-493, 2007.
- [22] Z. Huimin and Y. Wenyong, "An attitude determination method based on UKF and optimal REQUEST double filter," in *Artificial Intelligence, Management Science and Electronic Commerce (AIMSEC), 2011 2nd International Conference on*. IEEE, 2011, pp. 5377-5380.
- [23] Y. Cheng and J. Crassidis, "Particle filtering for sequential spacecraft attitude estimation," in *AIAA Guidance, Navigation, and Control Conference and Exhibit*, 2004, pp. 16-19.
- [24] M. Koifman and I. Bar-Itzhack, "Inertial navigation system aided by aircraft

- dynamics." *Control Systems Technology, IEEE Transactions on*, vol. 7, no. 4, pp. 487–493, jul 1999.
- [25] O. Hegrenaes, E. Berglund, and O. Hallingstad, "Model-aided inertial navigation for underwater vehicles," in *Robotics and Automation, 2008. ICRA 2008. IEEE International Conference on*, 2008, pp. 1069–1076.
- [26] X. Ma, S. Sukkarieh, and J. Kim, "Vehicle model aided inertial navigation," in *Intelligent Transportation Systems, 2003. Proceedings. 2003 IEEE*, vol. 2. IEEE, 2003, pp. 1004–1009.
- [27] M. Bryson and S. Sukkarieh, "Vehicle model aided inertial navigation for a UAV using low-cost sensors," in *Proceedings of the Australasian Conference on Robotics and Automation*, 2004.
- [28] J. Vasconcelos, C. Silvestre, and P. Oliveira, "Embedded vehicle dynamics and LASER aiding techniques for inertial navigation systems," in *Proceedings of the AIAA Guidance, Navigation, and Control Conference (GNC2006). Keystone, Colorado, USA. Citeseer*, 2006.
- [29] R. da Paixao, P. Rosa, and J. Neto, "An attitude heading and reference system: basic concepts and prototype," in *Industrial Electronics (ISIE), 2011 IEEE International Symposium on*, june 2011, pp. 2225–2230.
- [30] J. Guerrero-Castellanos, H. Madrigal-Sastre, S. Durand, N. Marchand, W. Guerrero-Sanchez, and B. Salmeron, "Design and implementation of an attitude and heading reference system (AHRS)," in *Electrical Engineering Computing Science and Automatic Control (CCE), 2011 8th International Conference on*, oct. 2011, pp. 1–5.

- [31] D. Gebre-Egziabher, R. Hayward, and J. Powell, "Design of multi-sensor attitude determination systems," *Aerospace and Electronic Systems, IEEE Transactions on*, vol. 40, no. 2, pp. 627-649, april 2004.
- [32] R. Munguia and A. Grau, "An attitude and heading reference system (AHRS) based in a dual filter," in *Emerging Technologies Factory Automation (ETFA), 2011 IEEE 16th Conference on*, sept. 2011, pp. 1-8.
- [33] P. Batista, C. Silvestre, P. Oliveira, and B. Carneira, "Low-cost attitude and heading reference system: filter design and experimental evaluation," in *Robotics and Automation (ICRA), 2010 IEEE International Conference on*, may 2010, pp. 2624-2629.
- [34] M. W. Ryan and G. Miller, "MEMS based AHRS with adaptive bias estimation for high performance rate sensor replacement," in *Position Location and Navigation Symposium (PLANS), 2010 IEEE/ION*, may 2010, pp. 214-220.
- [35] K. Britting, *Inertial navigation systems analysis*. Wiley-Interscience, 1971.
- [36] "IEEE standard for inertial systems terminology," *IEEE Std 1559-2009*, 26 2009.
- [37] G. Wahba, "Problem 65-1: A least squares estimate of satellite attitude," *Siam Review*, vol. 7, no. 3, p. 409, 1965.
- [38] F. Markley, "Fast quaternion attitude estimation from two vector measurements," *Journal of Guidance, Control, and Dynamics*, vol. 25, no. 2, pp. 411-414, 2002.
- [39] R. Hibbeler, *Engineering Mechanics: Dynamics*. Prentice Hall, 2009.
- [40] W. Phillips, *Mechanics of Flight*, 2nd ed. John Wiley & Sons, 2009.
- [41] L. Ljung, *System Identification: Theory for the User*. Pearson Education, 1998.

- [42] G. Welch and G. Bishop, "An introduction to the Kalman filter," *Design*, vol. 7, no. 1, pp. 1-16, 2001.
- [43] "ADIS16364 data sheet," Analog Devices, Inc., Norwood, MA, 2011.
- [44] G. Campa, "Airlib," 2003. [Online]. Available: <http://www.mathworks.com/matlabcentral/fileexchange/3019>
- [45] V. Scordamaglia, "Trajectory and attitude plot," 2004. [Online]. Available: <http://www.mathworks.com/matlabcentral/fileexchange/5656>
- [46] "MicroPilot," 2012. [Online]. Available: <http://www.micropilot.com/>



